Tumor immunology

Basic

Research Article

cDC2 plasticity and acquisition of a DC3-like phenotype mediated by IL-6 and PGE2 in a patient-derived colorectal cancer organoids model

Beatriz Subtil[1], Iris A. E. van der Hoorn[#1,2] (ID),
Jorge Cuenca-Escalona[#1] (ID)*, Anouk M. D. Becker[#1], Mar Alvarez-Begue[1],*
Kirti K. Iyer[1,3], Jorien Janssen[3] (ID)*, Tom van Oorschot[1], Dennis Poel[1,3]* (ID)*,*
Mark A. J. Gorris[1] (ID)*, Koen van den Dries[1], Alessandra Cambi[1],*
Daniele V. F. Tauriello[1,4] (ID) *and I. Jolanda M. de Vries[1]*

[1] Department of Medical BioSciences (MBS), Radboud University Medical Center, Nijmegen, the Netherlands

[2] Department of Pulmonary Diseases, Radboud University Medical Center, Nijmegen, the Netherlands

[3] Department of Medical Oncology, Radboud University Medical Center, Nijmegen, the Netherlands

[4] Department of Medical Oncology, Erasmus MC Cancer Institute, University Medical Center Rotterdam, the Netherlands

Metastatic colorectal cancer (CRC) is highly resistant to therapy and prone to recur. The tumor-induced local and systemic immunosuppression allows cancer cells to evade immunosurveillance, facilitating their proliferation and dissemination. Dendritic cells (DCs) are required for the detection, processing, and presentation of tumor antigens, and subsequently for the activation of antigen-specific T cells to orchestrate an effective antitumor response. Notably, successful tumors have evolved mechanisms to disrupt and impair DC functions, underlining the key role of tumor-induced DC dysfunction in promoting tumor growth, metastasis initiation, and treatment resistance. Conventional DC type 2 (cDC2) are highly prevalent in tumors and have been shown to present high phenotypic and functional plasticity in response to tumor-released environmental cues. This plasticity reverberates on both the development of antitumor responses and on the efficacy of immunotherapies in cancer patients. Uncovering the processes, mechanisms, and mediators by which CRC shapes and disrupts cDC2 functions is crucial to restoring their full antitumor potential. In this study, we use our recently developed 3D DC-tumor co-culture system to investigate how patient-derived primary and metastatic CRC organoids modulate cDC2 phenotype and function. We first demonstrate that our collagen-based system displays extensive interaction between cDC2 and tumor organoids. Interestingly, we show that tumor-corrupted cDC2 shift toward a CD14+ population with defective expression of maturation markers, an intermediate phenotype positioned between cDC2 and

---

Correspondence: Dr. I. Jolanda M. de Vries
e-mail: jolanda.devries@radboudumc.nl

[#]Iris A. E. van der Hoorn, Jorge Cuenca-Escalona, and Anouk M. D. Becker shared second co-authorship.

monocytes, and impaired T-cell activating abilities. This phenotype aligns with the newly defined DC3 (CD14$^+$ CD1c$^+$ CD163$^+$) subset. Remarkably, a comparable population was found to be present in tumor lesions and enriched in the peripheral blood of metastatic CRC patients. Moreover, using EP2 and EP4 receptor antagonists and an anti-IL-6 neutralizing antibody, we determined that the observed phenotype shift is partially mediated by PGE2 and IL-6. Importantly, our system holds promise as a platform for testing therapies aimed at preventing or mitigating tumor-induced DC dysfunction. Overall, our study offers novel and relevant insights into cDC2 (dys)function in CRC that hold relevance for the design of therapeutic approaches.

Additional supporting information may be found online in the Supporting Information section at the end of the article.

Introduction

Colorectal cancer (CRC) poses a significant global health burden, with high and increasing incidence and mortality rates [1, 2]. Particularly, advanced or metastatic CRC is associated with a poor prognosis and low 5-year survival rates, in part due to the inherent resistance of advanced CRC to conventional treatments and immunotherapeutic approaches [3, 4]. This highlights the urgent need for new and more effective therapies to reduce the morbidity and mortality associated with this disease.

Tumor progression and therapy resistance are closely intertwined with immune dysfunction. The tumor and its microenvironment (TME) shape and corrupt immune cells' phenotype and function, compromising immunosurveillance and antitumor immunity [5–7]. These effects extend to dendritic cells (DCs) — central components of the immune system — which are critically impaired in CRC patients, both locally at the tumor site and systemically [8]. Within the TME, properly functioning DCs are required for capturing, processing, and subsequently presenting tumor antigens to activate antigen-specific T cells and mount an efficient antitumor response. Moreover, DCs are also responsible for regulating immune responses by tuning the balance between immune activation and tolerance [9, 10].

Tumor-induced DC impairments have repercussions on the induction, regulation, and maintenance of effective antitumor immunity. Consequently, these impairments contribute to tumor progression, metastasis initiation, and immunotherapy resistance [8]. Strategies aimed at restoring DC function have shown promise in preclinical and clinical studies, highlighting the key role of DCs in cancer progression and the potential of targeting DCs as a therapeutic strategy, as extensively reviewed before [8, 11].

Malfunctioning DCs can have different roles and impacts on cancer immunity, depending on their subset [12]. Currently, four DC subsets are defined based on distinct ontogeny, phenotype, and functional specialization [12]. Namely, conventional dendritic cells type 1 and 2 (cDC1 and cDC2), specialized in inducing cytotoxic (CD8) and T-helper (CD4) T-cell responses, respectively; plasmacytoid dendritic cells (pDC) focused on type I interferon-mediated responses; and, DC3, a recently defined subset, closely related to cDC2. The developmental origin, functional properties, and role in (patho)physiological conditions of DC3 are still under debate and investigation [13–20].

Across several tumors, cDC2 are the most abundant DC subset [21, 22]. cDC2 greatly contribute to tumor immunosurveillance by inducing helper T-cell differentiation, but also by cross-presenting antigens [21]. Importantly, this subset has also been shown to be the most heterogeneous — functionally and phenotypically — and to present high susceptibility to TME-induced plasticity [23]. This heterogeneity and plasticity account for the dual pro- and antitumorigenic roles described for this subset of cancer [21].

Over the years, a cell population — often classified as a subpopulation of cDC2 — has gained attention due to its co-expression of cDC2 markers (CD1c) and monocyte/macrophage markers (CD14 and CD163). This population has been consistently found in tumors and peripheral blood of cancer patients, including breast, lung, colorectal, and ovarian cancers, as well as, melanoma and leukemia [12, 24–28]. Notably, this cell population has been associated with unfavorable prognosis, reduced overall survival, and low efficacy of immunotherapies [24, 27–29]. Interestingly, this cell population aligns with the recently defined DC3 subset, characterized by an intermediate transcriptomic and phenotypic profile between cDC2 and monocytes (CD1c$^+$ CD14$^+$ CD163$^+$ DCs); DC3 exhibits distinct functionality from both but bears closer relation to cDC2.

Recent studies indicate that DC3 emerges from a separate DC lineage with an independent precursor and a distinct ontogeny profile compared with monocytes and cDC2 [14, 21, 25, 29–34]. However, previous in vitro studies suggest that a similar population (often referred to as CD1c$^+$ CD14$^+$ cells or CD14$^+$ cDC2) can arise from human cDC2 when exposed to tumor cells,

tumor-conditioned medium, or (tumor-derived factors) such as IL-6, prostaglandin E2 (PGE2), and M-CSF in 2D and 3D settings [28, 35]. As of now, the relationship between the DC3 arising from separate progenitors and the comparable population originating from cDC2 (in vitro) remains uncertain, giving rise to nomenclature challenges and inconsistencies within the field's literature.

All in all, given the abundance, heterogeneity, and plasticity of cDC2 within tumor settings, it remains imperative to uncover the impact of CRC, and corresponding mediators, on the fate, phenotype, and functions of cDC2. Understanding the mechanisms that regulate the fate of cDC2 within the CRC TME, will be pivotal to define strategies to tackle and revert tumor-induced cDC2 dysfunction, and subsequently unleash antitumor immunity and treatment responsiveness.

In order to gain more insight into the impact of CRC-driven immunosuppression on cDC2, we employ our recently developed 3D co-culture system featuring (primary and metastatic) CRC patient-derived tumor organoids (PDTOs) [36, 37]. In our previous work involving human monocyte-derived DCs, we have been able to detect the suppressive influence of PDTOs on the phenotype, behavior, and function of these ex vivo differentiated DCs [36]. PDTOs represent a powerful and relevant tumor model, consisting of self-assembling 3D cellular structures derived from tumor samples. These structures faithfully recapitulate key aspects of the patient's disease, including genetic heterogeneity and response to therapy [37–41]. Additionally, we use primary cDC2 (CD1c$^+$ CD14$^-$) derived from the blood of healthy donors. Moreover, to ensure clinical relevance, we study and detect the presence of cDC2 populations in the blood and tissue of metastatic CRC patients. With this toolbox, we aim to contribute to the unveiling of the intricacies of cDC2 phenotypic, behavioral, and functional plasticity within the context of CRC. Our study also seeks to identify key mediators involved in shaping these processes, to inform the design of new therapeutic approaches.

Materials and methods

Healthy donor/patient blood and tissue samples

Blood samples — buffy coats and heparin tubes — from healthy donors were obtained via Sanquin Blood Bank (Sanquin Bloedvoorziening). Collection and use of blood samples from metastatic CRC patients were approved by the local medical ethical committee of the Radboudumc (local registration 2021–13248) (not WMO compulsory). Tumor tissue sections from primary tumors and liver metastasis of CRC patients were obtained within the context of the ORCHESTRA trial (NCT01792934). All healthy donors and patients gave written informed consent.

Isolation of peripheral blood mononuclear cells

Peripheral blood mononuclear cells (PBMCs) were isolated from buffy coats and heparin blood tubes by density gradient cen-

trifugation using Lymphoprep medium (StemCell Technologies, 07861). The residual red blood cells were removed using red blood cell lysis buffer (Gibco, A1049201). From the obtained PBMC fraction, cDC2 and Pan T cells were isolated as described below.

Isolation of conventional dendritic cells type 2

cDC2 (CD1c$^+$ CD14$^-$) cells were purified with magnetic cell sorting from PBMCs using the CD1c (BDCA1$^+$) DC isolation kit (Miltenyi Biotec, 130-119-475) according to the manufacturer's instructions. cDC2 purity was assessed by flow cytometry based on CD1c-BV421 (331526, Biolegend), CD14-APC-H7 (560180, BD Biosciences), CD20-FITC (2168194, BD Biosciences), and CD3-PE (3135936, BD Biosciences) staining (Supporting information Fig. S1). Following isolation, cDC2 (>95% pure) were directly incorporated into the co-culture system.

Isolation of Pan T cells

Pan T cells were isolated from the peripheral blood lymphocyte fraction of the PBMCs by depletion of non-T cells with magnetic cell sorting using the Pan T-cell isolation kit (Miltenyi Biotec, 130-096-535) according to the manufacturer's instructions.

Patient-derived tumor organoids

In this study, PDTOs derived from three patients with metastatic CRC and composed exclusively of (epithelial) tumor cells were used. Two PDTOs from liver metastasis (PDTO LM) were developed and cultured as previously described [36, 37]. PDTO LM (2) in this study corresponds to PDTO013 as originally named in the biobank [37] and to PDTO cystic in our previous study [36]. PDTO LM (3) in this study corresponds to PDTO024 as originally named in the biobank [37] and to PDTO dense in our previous study [36].

The other two PDTOs were obtained via the Hubrecht Organoid Technology (HUB) Institute under the license and request MTA Radboudumc OSR-2021-012. Both PDTOs are derived from the same patient, from samples of the primary colon tumor — in this study named PDTO PC (1), original identification code HUB-02-B2-031 — and of the liver metastasis — in this study named PDTO LM (1), original identification code HUB-02-C2-031. The organoids were defrosted and cultured according to the provider's instructions.

Generation of co-cultures between PDTOs and cDC2 in a 3D collagen gel

The scaffold used for the 3D co-culture system was Bovine Collagen type I. The collagen mix was neutralized and prepared as

described before [36, 42]. PDTOs, carefully collected to avoid mechanical fragmentation (in a volume corresponding to the desired amount of counted cells in another identical sample) and freshly isolated cDC2 were embedded in the collagen mix in a ratio of 1:1 (60,000:60,000 cells) per each 25 μL dome, as previously described [36]. For each condition, two 25 μL domes were added per well in a 24 wells-plate. The collagen gels were polymerized, with the plates inverted, for 45 min at 37°C. The co-cultures were incubated for 48 h in X-VIVO 15 (BE02-060F, Lonza) supplemented with 2% human serum. Co-culture supernatants were collected at 48 h and stored at −20°C.

Inhibitors and modulators of secretome within the 3D co-culture

To modulate the secretome and target IL-6 and PGE2 activity, 5 μg/mL of anti-IL-6 neutralizing antibody (Invivogen, 6446-430) and 120 μM of EP2 (Cayman chemicals, AH6809 14050) and 6 μM of EP4 (Cayman chemicals, L161982 10011565-5) receptor antagonists were added at 24 h of co-culture [35, 43]. A solvent control condition was included containing the corresponding amounts of MiliQ water and DMSO used to dissolve the inhibitor/antagonists.

Cell labeling and live imaging of the 3D co-culture

For advanced light imaging, cDC2 were labeled with CellBrite Red cytoplasmic membrane dye (30023, Biotium) and PDTOs were labeled with CellBrite Green cytoplasmic membrane dye (30021, Biotium) according to the manufacturer's instructions, immediately prior to the generation of the co-cultures. The percentage of viable cDC2 within the 3D collagen gels was assessed by using simultaneously the CellBrite Red dye and ReadyProbes Cell Viability Imaging Kit (ThermoFisher, R37609), at 2, 24, and 48 h of co-culture. The microscope Zeiss Axio Observer (5× and 10× magnification) and Ibidi μ-Plate 24 Well Black ID 14 mm were used for imaging. For time series, images were taken every 1 min. Images and time-lapses were processed, adjusted, and analyzed using ImageJ.

Immunofluorescence in 3D collagen gels

For 3D immunofluorescence stainings, the co-cultures were fixed for 1h with 4% PFA and then blocked (20 mM glycine, 2% BSA, and 0.3% Triton in phosphate buffer) for 1 h at room temperature. After the washing steps, primary antibodies were added: 1:300 rabbit anti-CD11c (Abcam, ab52632) and 1:100 mouse anti-pan-cytokeratin (Abcam, ab7753), and the samples were incubated overnight at 4°C in a humidified chamber. The following day, secondary antibodies were added: donkey anti-rabbit 488 (Invitrogen, A21206), donkey anti-mouse 647 (Invitrogen, A31571) both 1:200 and 2.5 μg/ml DAPI (Roche, 10236276001). Samples

were mounted with Fluoromount-G (SouthernBiotech, 0100–01). Once dry, the slides were imaged with a Zeiss confocal laser scanning microscope LSM880. Image processing was performed using Image J.

Paraffinization and slide preparation

For immunohistochemistry stainings, samples were prepared by fixing the co-cultures in Formalin for 1 h. The samples were then placed in a Sakura Tissue-Tek Paraform cassette and embedded in paraffin. The formalin-fixed, paraffin-embedded co-cultures were sectioned into 4 μm slides with a microtome (Microm).

Triplex immunohistochemistry in co-culture tissue and imaging

The co-culture slides were stained using the Opal 6-Plex Detection Kit (Akoya Biosciences, NEL861001KT) on the Leica Bond system (BOND-Rx Fully Automated IHC and ISH, Leica Biosystem) as previously described [44, 45]. Antibodies directed against 1:100 CD1c (Abcam, ab156708) — Opal 520, 1:200 CD14 (Cell Signaling, 75181S) — Opal 620, and 1:1500 pan cytokeratin (Abcam, ab86734) — Opal 650 were used. Cell nuclei were counterstained using DAPI (NEL797B001KT, PerkinElmer) at room temperature for 5 min, after which slides were enclosed using Fluoromount-G (Southern Biotech, 0100–01). Image acquisition was performed on the Vectra Polaris Automated quantitative Pathology Imaging System (PerkinElmer), after which the multispectral images were unmixed in inForm Advanced Image Analysis Software (inForm 2.4.8, PerkinElmer).

Multiplex immunohistochemistry in patient samples and imaging

The patient slides were stained using the Opal 7-color automation IHC kit (Akoya Biosciences, NEL801001KT) on the Leica Bond system (BOND-Rx Fully Automated IHC and ISH, Leica Biosystem) as previously described [44, 46]. The multiplex panel consisted of 1:200 anti-CD14 (Cell Marque, 114R-16) — Opal 620, 1:200 anti-CD19 (Abcam, ab134114) — Opal 690, 1:150 anti-BDCA2 (Dendritics, DDX0043) — Opal 540, 1:100 anti-CD1c (Thermo Fisher Scientific, TA505411) — Opal 520, 1:100 XCR1 (Cell Signaling Technologies, 44665S) — Opal 570 and 1:1500 anti-pan cytokeratin (Abcam, ab86734) — Opal 650. Cell nuclei were counterstained using DAPI (NEL797B001KT, PerkinElmer) at room temperature for 5 min, after which slides were enclosed using Fluoromount-G. Whole tissue slides were imaged using the microscope Vectra 3 Automated Quantitative Pathology Imaging System (Version 3.0.4, PerkinElmer Inc.). For this study, only DAPI, CD1c, CD14, and pan-cytokeratin channels are shown.

Table 1. Overview of anti-human antibodies used to stain PBMCs for flow cytometry.

Marker	Fluorochrome	Company	Catalog number	Dilution
HLA-DR	PerCP	BioLegend	307628	1:25
CD141 (BDCA3)	APC	Miltenyi	130-113-314	1:25
CD14	APC-H7	BD Biosciences	560180	1:25
CD1c (BDCA1)	PE	Miltenyi	130-113-302	1:25
CD3	FITC	BD Biosciences	555339	1:25
CD20	FITC	BD Biosciences	345792	1:25
CD19	FITC	BD Biosciences	555412	1:25
CD56	FITC	BD Biosciences	562794	1:25

Flow cytometry, antibodies, and staining of cells in blood of patients and healthy donors

PBMCs isolated from blood samples of metastatic CRC patients or healthy donors were stained to assess the percentage of cDC2 (CD1c$^+$) — CD14$^+$ or CD14$^-$ populations. Firstly, samples were stained with Zombie Green fixable viability kit (Biolegend, 423111) according to the manufacturer's instruction. Second, Fc receptors were blocked using Fc blocking reagent (Miltenyi, 130-059-901) for 10 min at 4°C. Thirdly, directly labeled primary antibodies were added for 25 min at 4°C (Table 1). The acquisition was performed on a FACSLyric flow cytometer (BD Biosciences). The acquired data were analyzed with FlowJo Version 10. The values were plotted as a percentage of positive cells.

3D co-culture dissociation

For collagen dissolution and co-culture disaggregation, Collagenase I (Sigma-Aldrich, C0130) was added to the co-culture medium (100 U/mL) and incubated until dissolution at 37°C. The cell suspension was collected and cDC2 viability was assessed using trypan blue and BIO-RAD TC20 Automated Cell Counter (prior to centrifugation). Samples were washed — and the ones containing PDTOs were filtered through a Corning Cell Strainer (70 μm Nylon MESH) — before staining and acquisition by flow cytometry or sorting.

Flow cytometry and sorting: antibodies and staining of cells in collagen co-cultures

Phenotypic characterization of cDC2 surface markers was performed as follows: Fc receptors were blocked using Fc blocking reagent (Miltenyi, 130-059-901) for 10 min at 4°C, and then directly labeled primary antibodies were added for 25 min at 4°C (Table 2). The acquisition was performed on a FACSVerse flow cytometer (BD Biosciences). The acquired data were analyzed with FlowJo Version 10. The values were plotted as raw data, percentage of positive cells, or fold change/normalized geometric mean fluorescence intensity (MFI). Relevant gating strategies

used are depicted in the Results or Supporting information Data sections. cDC2 were sorted based on CD1c (and CD14) expression (Table 2), for functional readouts with T cells using the BD FACSMelody cell sorter (BD Biosciences).

Allogenic T-cell proliferation assay: mixed lymphocyte reaction

The ability of cDC2 to induce T-cell proliferation was assessed in mixed lymphocyte reactions using allogenic T cells. Sorted cDC2 were seeded in triplicates with CFSE (Invitrogen, C34554)-labeled Pan T cells in a 1:10 ratio for 5 days. On day 6, T cells were collected and stained with anti-CD8-APC (BD Biosciences, 555369), 1:30, for 25 min at 4°C. T-cell proliferation was assessed based on the percentage of CFSE-negative cells. Samples were acquired using FACSVerse flow cytometer and analyzed with FlowJo Version 10. Co-culture supernatants were collected on day 6 and stored at −20°C.

Flow cytometry-based multiplex cytokine array and ELISAs

Quantification of soluble factors in supernatants of cDC2 and PDTOs co-cultures was assessed using a flow cytometry-based cytokine assay — LEGENDplex Human Inflammation Panel 1 (13-plex) (Biolegend, 740809). Complementarily, M-CFS (Invitrogen, EHCSF1) and PGE2 (Invitrogen, KHL1701) ELISAs were performed. For the supernatants of cDC2 and Pan T-cell co-cultures a subpanel of the aforementioned 13-plex was used.

Statistical analysis

The statistical analysis was performed using GraphPad Prism V10 (GraphPad Software Inc.). The specific statistical test applied is specified in the Figures' legends. Unless otherwise indicated, results are presented as mean ± SD in scattered dot plots. The statistical significance was annotated as follows: $*p < 0.05$, $**p < 0.01$, $***p < 0.001$, $****p < 0.0001$.

Table 2. Overview of anti-human antibodies used to stain cDC2 for flow cytometry and fluorescent-activated cell sorting.

Marker	Fluorochrome	Company	Catalog number	Dilution
HLA-DR	PerCP	BioLegend	307628	1:30
MerTK	PE-Cy7	BioLegend	367609	1:50
CD86	APC	BD Biosciences	555660	1:50
CD14	APC-H7	BD Biosciences	560180	1:30
CD1c	PE	Miltenyi	130-113-302	1:50
CD163	BV421	BD Biosciences	562643	1:30
CD11b	FITC	Invitrogen	11-0118-42	1:50
CD5	FITC	Invitrogen	11-0058-42	1:100

Results

Overview of the 3D co-culture system: morphology of CRC PDTOs and cDC2 viability

In this study, cDC2 was cultured alone or together with PDTOs for 48 h in a 3D collagen gel, similar to our previously developed 3D co-culture system (Fig. 1A) [36]. To investigate the effects of primary and metastatic CRC PDTOs on cDC2 phenotype and function four different PDTOs were used. Two organoids were derived from the same patient from the colon primary tumor site [PDTO CP (1)] and the liver metastasis [PDTO LM (1)], and two were derived from liver metastasis of two other patients [PDTO LM (2) and (3)]. These organoids present distinct morphologies ranging from cystic to dense/compact forms (Fig. 1B).

The viability of cDC2 was assessed through live imaging using a cell tracking dye, together with DAPI and a cell death dye (Fig. 1C). Overall, there were no significant differences in cDC2 viability whether cultured alone or with PDTOs (Fig. 1D). While the viability gradually declined over the course of 48 h (70–80% after 24 h and 60–70% after 48 h), this decline was comparable across all conditions. Moreover, 3D viability scores resembled those in 2D settings (Fig. 1D). Thus, co-culture with PDTOs in a 3D setting does not seem to compromise the viability of cDC2.

Interactions between cDC2 and CRC PDTOs

After establishing the viability of our co-culture system, we aimed to explore and characterize the interactions between cDC2 and PDTOs within the 3D context. Using advanced light microscopy and live imaging, we visualized the dynamic and direct interactions between cDC2 and PDTOs in the 3D collagen gel. Notably, cDC2 migrated toward, clustered around, and infiltrated the PDTOs (Fig. 2; Supporting information Fig. S2 and Supporting information Movies S1–S8). Interestingly, cDC2 were often found in the proximity of dead tumor cells, as well as surrounding tumor cells or fragments (Fig. 2B and D; Supporting information Fig. S2).

Identification of a CD14$^+$ cDC2 population within the 3D co-culture and in patient samples

We next evaluated the impact of the PDTOs on the cDC2 phenotype and function. For this, cDC2 were first retrieved from the 3D co-culture using collagenase (Supporting information Fig. S3A). The viability of cDC2 after the collagenase treatment (60–70%, Supporting information Fig. S3B) was comparable to values obtained from microscopy images before retrieval (Fig. 1D). Upon recovery from the matrix, cDC2 were stained for flow cytometry and gated for phenotypic analysis based on HLA-DR and CD1c expression (Supporting information Fig. S3C). The activation markers (CD86) and the major histocompatibility complex (MHC) class II cell surface receptor (HLA-DR) were slightly upregulated in the presence of PDTOs (Supporting information Fig. S3D). In line with this, the ability of cDC2 to induce T-cell proliferation was increased in the presence of PDTO LM (2) in comparison to cDC2 cultured alone (Supporting information Fig. S3E). Increased T-cell proliferation coincided with higher production of IFN-γ and TNF-α by T cells (Supporting information Fig. S3F).

To assess the degree of tumor-induced phenotypic plasticity in cDC2, we also analyzed the expression of CD14. Interestingly, this marker was strongly increased in the presence of all PDTOs, with the corresponding histogram showing the appearance of a new population of CD14$^+$ cDC2 (Supporting information Fig. S3D). We confirmed this distinctive population by evaluating CD14 expression in CD1c-positive cells, as shown in Fig. 3A. The size of this population displayed a two- to four-fold increase in all the conditions with PDTOs, underscoring a tumor-driven effect (Fig. 3B). Among the PDTOs, PDTO LM (3) exhibited the lowest ability to induce the CD14$^+$ population.

The presence of the CD1c$^+$ CD14$^+$ cell population in the conditions with PDTOs was further corroborated by multiplex immunohistochemistry, where approximately half (46%) of the cells demonstrated clear co-expression of both markers (Fig. 3C and D; Supporting information Fig. S4). The spatial distribution of these CD14$^+$ cDC2 cells appeared homogenous, and not restricted to the direct vicinity of the tumor, implying that a soluble tumor-derived factor may be involved (Fig. 3C; Supporting information Fig. S4).

To further investigate the clinical relevance of this CD14$^+$ population, we examined tissue samples from CRC patients. Notably,
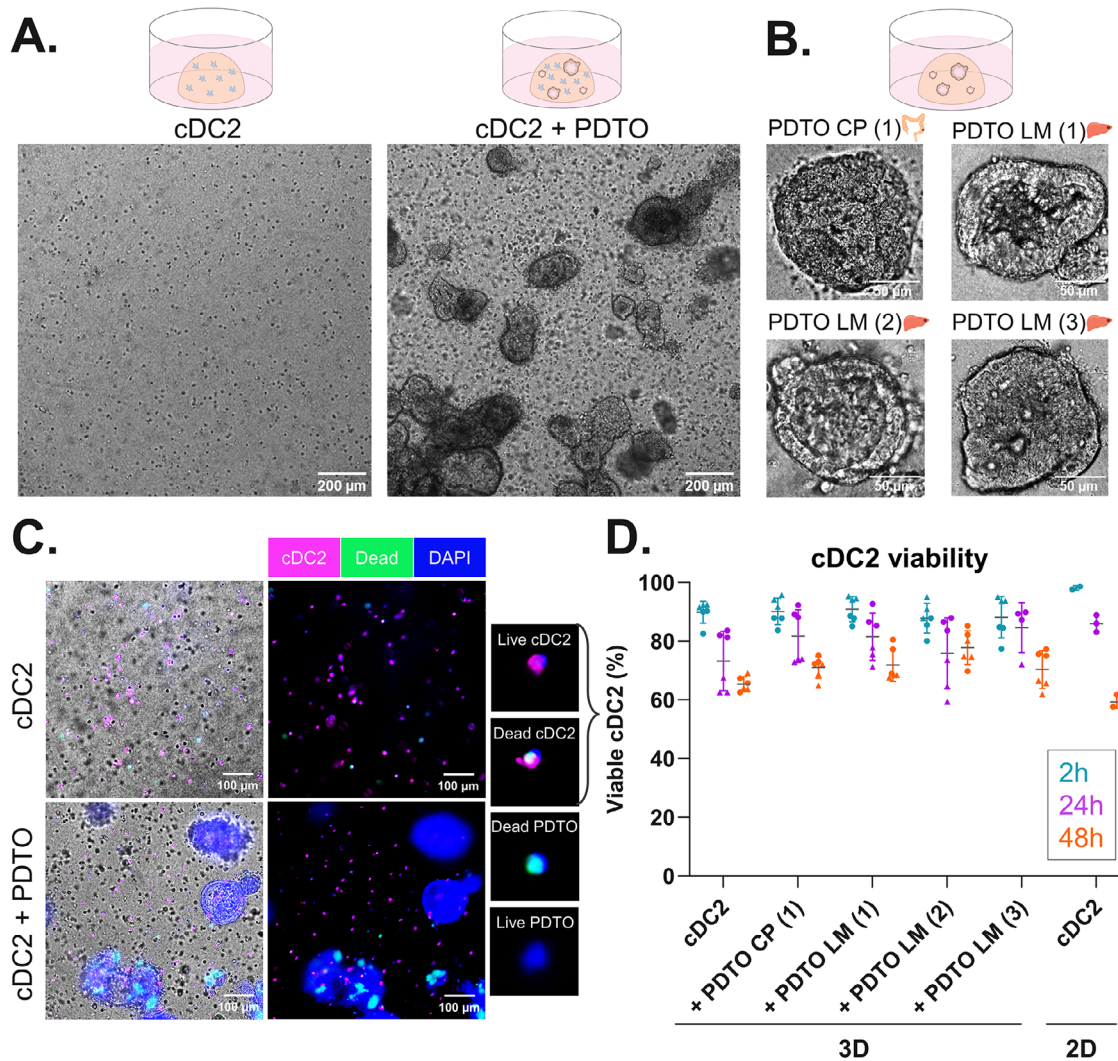
Figure 1. 3D co-culture system: overview, morphology, and viability quantification. (A) Overview of the co-culture system when cDC2 were cultured alone or in the presence of PDTOs in the 3D collagen gel. Images were acquired with the Axio Observer Zeiss microscope, 5× magnification. (B) Closeup of the different PDTOs used in this study cultured in the 3D collagen gel. PDTO CP (1) is derived from a primary colon tumor and PDTO LM (1), (2), and (3) are derived from CRC liver metastasis. Images acquired with a 10× magnification using the microscope Zeiss Axio Observer (C) Representation of the different stainings used to discern between live and dead cDC2 and PDTOs: CellBrite Red dye (cDC2 in magenta), NucBlue Live (live cells in blue) and NucGreen Dead (dead cells in green) stainings. (D) Quantification of the percentage of viable cDC2 in the different conditions. Two cDC2 donors were used for the 3D samples and one donor for the 2D sample. Three images per condition per donor were analyzed (each dot represents one image). Viability was assessed at 2, 24, and 48 h of co-culture.

cells co-expressing CD14 and CD1c were also found in both primary and metastatic CRC samples (Fig. 3E). Additionally, the percentage of circulating CD14+ cDC2, and not CD14− cDC2, was increased in the blood of metastatic CRC patients when compared with healthy donors (Fig. 3F).

Phenotypical and functional characterization of PDTO-induced CD14+ cDC2 and comparison to DC3

Given the tumor-related presence of the CD14+ cDC2 population in CRC, both within the co-culture system and in patients, we delved deeper into their phenotype and function. Following

the same workflow as before, we now analyzed both cDC2 populations separately to better define their phenotype (Fig. 4A). Furthermore, we isolated each subpopulation by fluorescence-activated cell sorting for subsequent functional assays (Fig. 4A).

Firstly, we looked at several markers, CD1c, CD14, CD163, CD5, CD86, HLA-DR, and MerTK, commonly used to characterize DC3 to determine if the CD14+ cDC2 generated within the co-culture system would resemble them. It became clear that the CD14+ and CD14− populations present differential expressions of the examined phenotypic markers. Interestingly, the CD14+ cDC2 population expressed high CD163, MerTK, and CD11b, and low HLA-DR, CD5, and CD86, which aligns with the DC3 subset
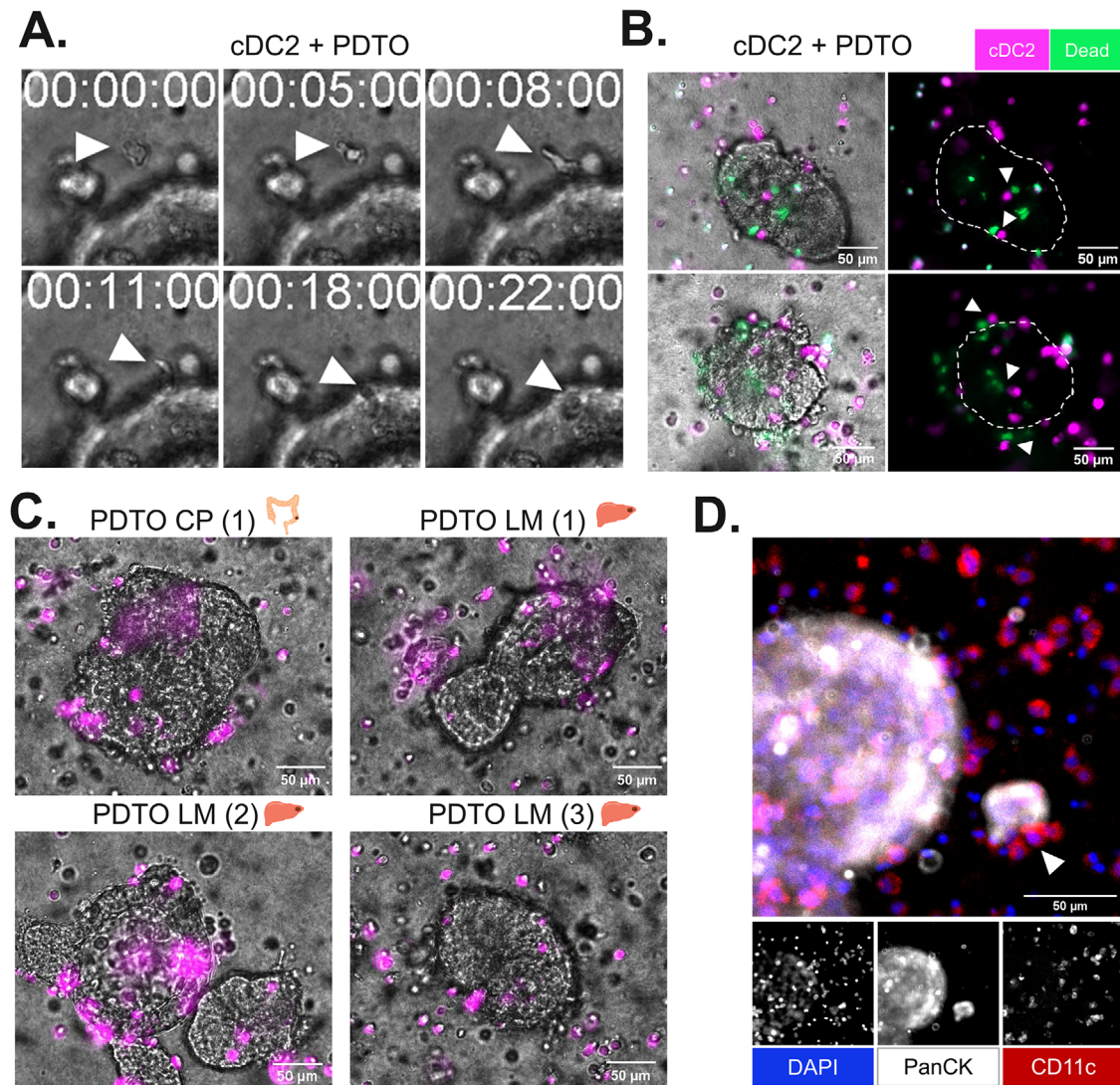
Figure 2. cDC2 and PDTOs interactions in the 3D co-culture system. (A) Closeup of a time-lapse movie showing a cDC2 moving toward and into a PDTO. Images were acquired with the Axio Observer Zeiss microscope, 10× magnification. (B) Examples of co-cultures displaying cDC2 (CellBrite Red dye) in magenta and dead cells (NucGreen Dead) in green. cDC2 surrounding and infiltrating the PDTOs, and near dead tumor cells as pinpointed by the arrows. (C) cDC2 (CellBrite Red dye) in magenta surrounding and infiltrating all the PDTOs used in this study. Corresponding movies can be found in Supporting information Data. (D) 3D immunofluorescence stainings (DAPI, CD11c, and PanCK) performed on fixed co-cultures, show cDC2 agglomerating around and possibly sampling tumor cells or tumor-derived fragments. (Of note, the DAPI-positive events, apparently lacking CD11c$^+$ labeling, correspond to cDC2 situated in a different optical plane, leading to a diminished fluorescent signal.) Images were acquired with a Zeiss confocal laser scanning microscope LSM880.

phenotype. Conversely, CD14$^-$ cDC2 showed the opposite pattern (Fig. 4B).

Secondly, we studied the impact of PDTOs on the CD14$^+$ and CD14$^-$ cDC2 populations specifically by gating them separately and comparing their respective tumor-induced phenotypes (Fig. 4A and C; Supporting information Fig. S5). Notably, the increased expression of CD86 and HLA-DR, previously observed (Supporting information Fig. S3D) only occurs within the CD14$^-$ population (Fig. 4C).

Thirdly, we assessed the ability of both sorted populations to induce T-cell proliferation and stimulate the release of proinflam-

matory cytokines (Fig. 4A, D, and E). Reflecting their phenotype, the CD14$^-$ negative fraction seems to be able to stimulate proliferation and secretion of pro-inflammatory cytokines by CD4 and CD8 T cells. In contrast, the CD14$^+$ population exhibited relatively impaired abilities in inducing T-cell proliferation and activation.

In summary (Fig. 5), the PDTOs: (1) induce a CD1c$^+$ CD14$^+$ CD163$^+$ cell population analogous to DC3, with impaired T-cell proliferating and activating abilities; (2) activate the remaining CD14$^-$ fraction, albeit in reduced numbers, which is able to effectively trigger T-cell proliferation and proinflammatory cytokine
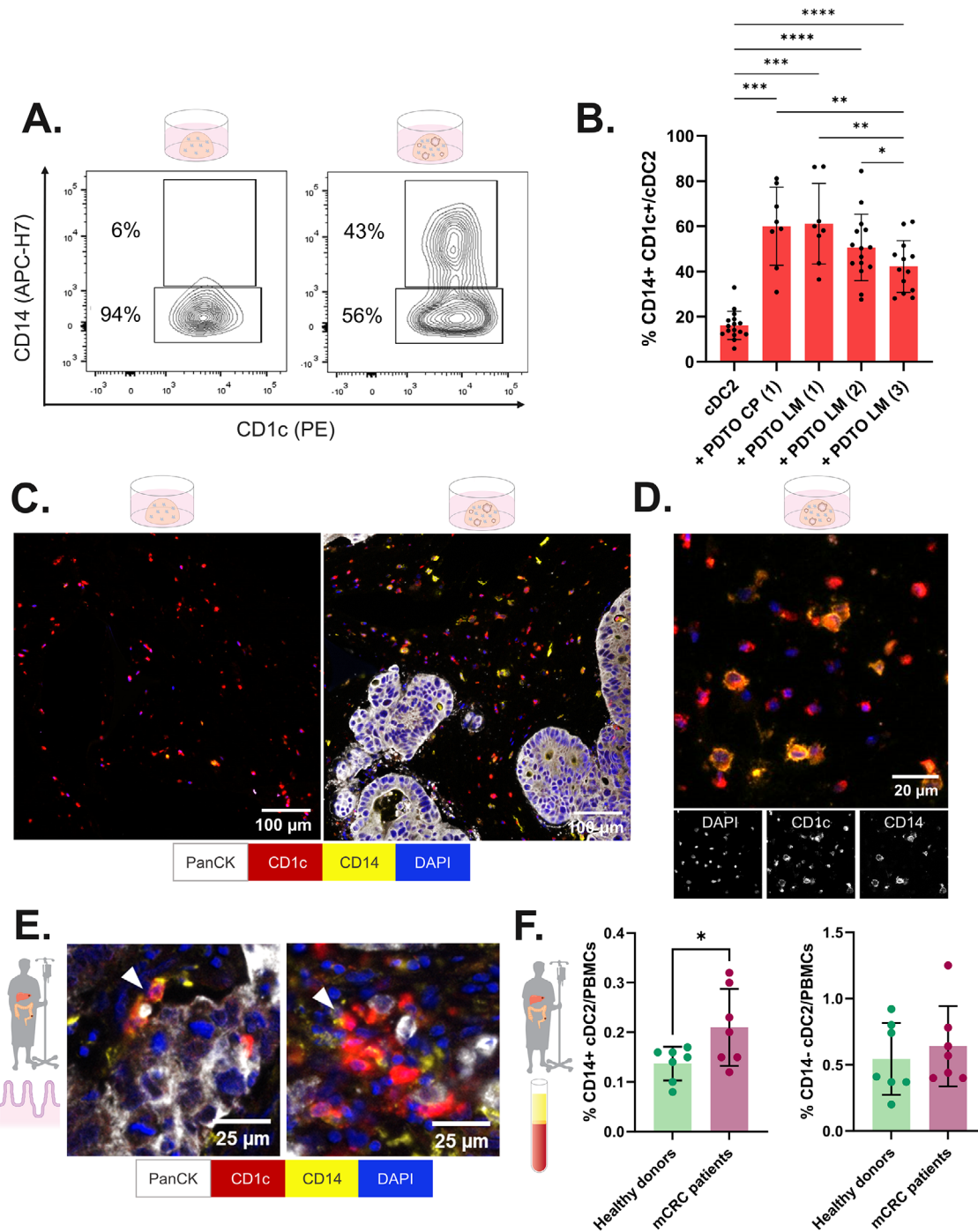
Figure 3. A CD14$^+$ cDC2 population arises upon co-culture with PDTOs, which is also present in circulation and at the tumor site of metastatic CRC patients. (A) Representative gating strategy, with contour plots, illustrating the arising of a CD1c$^+$ CD14$^+$ population in the presence of PDTOs. (B) The percentages of CD14$^+$ cells within the CD1c$^+$ (cDC2) population were gathered and plotted. Each dot represents a different cDC2 donor. The statistical significance was assessed by a mixed-effects model followed by a Dunnett's post hoc multiple comparisons test and annotated as follows: $^{***}p < 0.001$, $^{****}p < 0.0001$. (C) A 3-plex immunohistochemistry panel (PanCK, CD1c, and CD14) was used to stain slides of fixed co-cultures and confirm the presence of the CD1c$^+$ CD14$^+$ population. Images were acquired with Vectra Polaris Automated Quantitative Pathology Imaging System. (D) A closeup of a co-culture section stained shows the presence of CD1c$^+$ CD14$^+$ cells. (E) A multiplex immunohistochemistry panel (here only shown the PanCK, CD1c, and CD14 markers) was used to stain CRC patient tissue samples from liver metastasis and primary tumors. A closeup of sections confirms the presence of CD1c$^+$ CD14$^+$ cells (arrowheads) in the tumor site of these patients. (F) The percentage of CD14$^+$ and CD14$^-$ cDC2 (CD1c$^+$) within the PBMCs were assessed in blood samples from metastatic CRC patients ($n = 7$) and healthy donors ($n = 7$). Each dot represents a different donor/patient. The statistical significance between conditions was assessed by an unpaired t-test and annotated as $^*p < 0.01$.
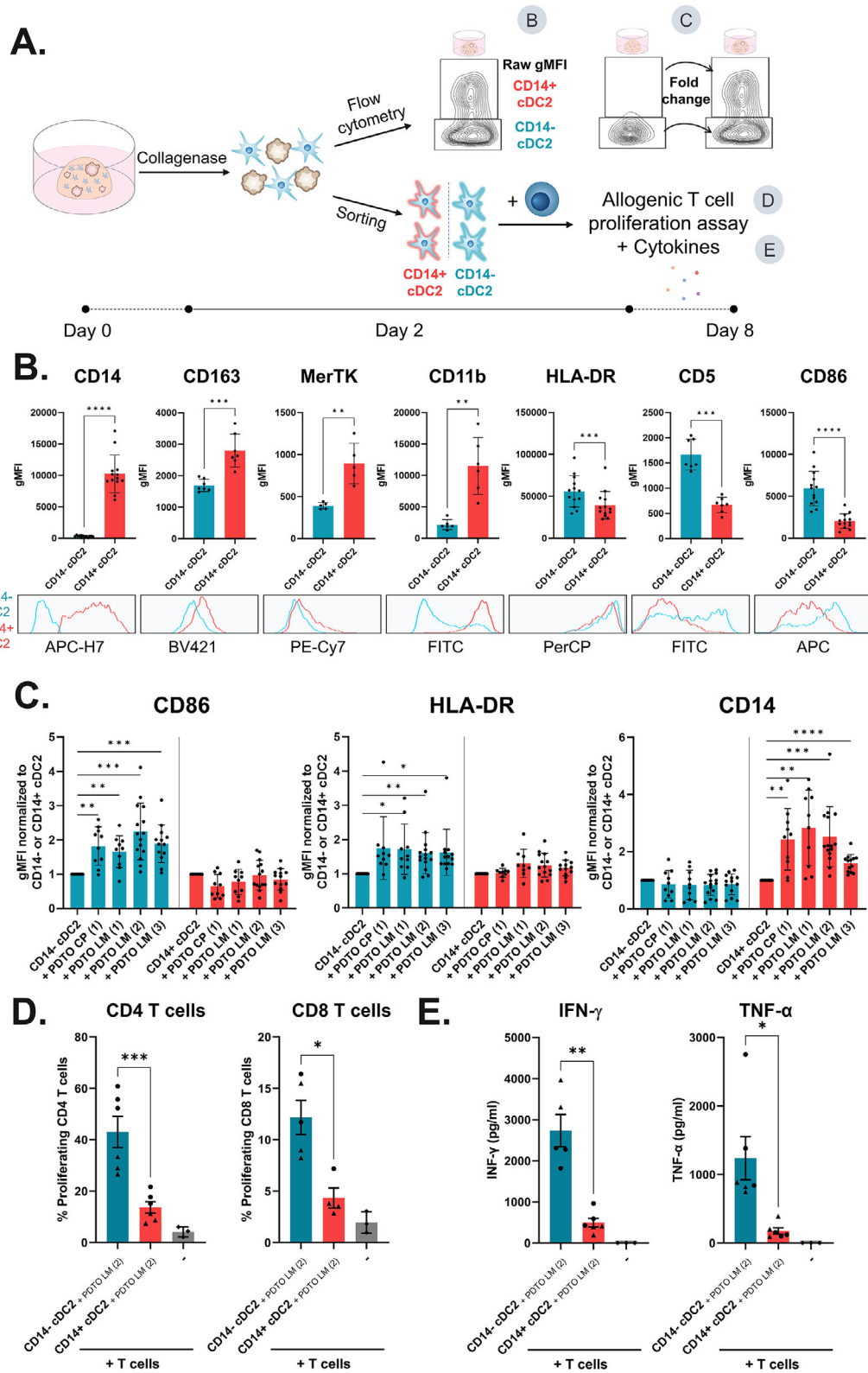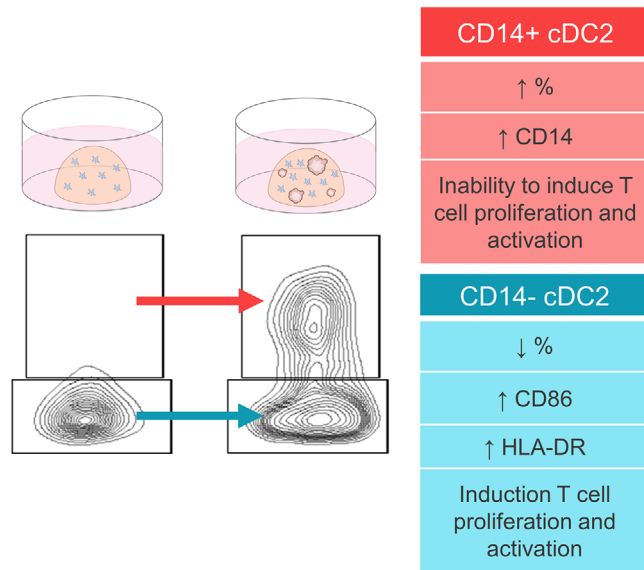
Figure 5. Summary and overview of the key effects of co-culture with PDTOs on the phenotype and function of CD14$^+$ and CD14$^-$ cDC2 populations.

secretion. We conclude that the PDTOs have a dual effect, steering the initial CD14$^-$ cDC2 population into two distinct phenotypes, highlighting cDC2 plasticity.

Conversion of cDC2 toward a DC3-like phenotype is partially mediated by PGE2 and IL-6

To determine whether and which soluble factors could potentially be involved in the cDC2 phenotype shift into DC3-like cells, we screened the supernatants of cDC2 and PDTO co-cultures for several tumor-related factors (Fig. 6A; Supporting information Fig. S6A). Noteworthy, most analyzed factors were secreted during co-culture and not when the cDC2 or the PDTOs were cultured alone in the 3D collagen. This suggests dynamic crosstalk between cDC2 and PDTOs. In addition, co-cultures with different PDTOs generated distinct secretome profiles.

Next, we aimed to determine if we could prevent the tumor-induced phenotype shift in CD14 expression. We directed our attention to two factors, namely IL-6 and PGE2, which were found to be expressed in the co-culture system (Fig. 6A) and have been

previously associated with the induction of this phenotype in different in vitro settings [28, 35]. Following a 24 h co-culture period, we added an anti-IL-6 antibody [35] or EP2 + EP4 receptor antagonists [43] to abrogate IL-6 and PGE2 activity, respectively (Fig. 6B).

We observed that PDTO CP (1), PDTO LM (1), and PDTO LM (2) responded similarly to the anti-IL-6 neutralizing antibody and EP2 + EP4 antagonists. At the concentrations used, both treatments induced a 20–40% decrease in the CD14+ cDC2 population compared with the untreated co-cultures. Interestingly, PDTO LM (3) did not respond to the anti-IL-6 neutralizing antibody, while treatment with the EP2 and EP4 antagonists led to a 40–60% decrease in the CD14$^+$ cDC2 population compared with the untreated co-cultures. These findings align with the observed lack of IL-6 expression by PDTO LM (3) and corroborate treatment specificity (Fig. 6A and C). In addition, our findings suggest that the combination treatment (EP2/EP4 antagonists + anti-IL-6 neutralizing antibody) does not lead to a cumulative effect (Supporting information Fig. S6B).

Even though after treatment CD14$^+$ cDC2 percentages were not restored to the levels of the cDC2 cultured alone, it seems possible to partially prevent the tumor-induced CD14$^+$ phenotype (Fig. 6C). Overall, our results suggest that IL-6 and PGE2 signaling contribute to and are involved in the conversion of cDC2 toward a DC3-like phenotype.

Discussion

The primary goal of this study was to gain a deeper understanding of the mechanisms that regulate the fate of cDC2-mediated antitumor responses or tolerance in CRC. To shed light on the CRC-driven cDC2 plasticity and (dys)function we exploited and adapted our previously developed 3D co-culture system, using both metastatic and primary CRC PDTOs [36]. The end goal of this research was to identify and test potential targets for cDC2-specific interventions, with the aim of preventing tumor-induced DC impairment, and ultimately restoring and unleashing antitumor immunity in CRC patients.

The main added value of this study is the 3D co-culture setup that allows the investigation of human primary cDC2 – phenotype, behavior, and function – in a patient-derived CRC organoid context. To our knowledge, this is the first study and model investi-

Figure 4. Phenotypic and functional characterization of the CD14$^+$ and CD14$^-$ cDC2 populations upon co-culture with PDTOs. (A) Schematic representation of the workflow followed to evaluate CD14$^+$ and CD14$^-$ cDC2 phenotype and function after co-culture with PDTOs. Letters correspond to the respective panels where results are depicted. (B) Scattered dot plots of raw geometric MFI, mean with SD, for each population when cDC2 were co-cultured with PDTOs. Each dot represents a different donor. Each plot is accompanied by a representative histogram. The statistical significance between conditions was assessed by a paired sample *t*-test. (C) The impact of the PDTOs on the CD14$^+$ and CD14$^-$ populations was evaluated separately by the fold change in MFI marker expression of these populations between the conditions without and with PDTOs. Data plotted as normalized values of raw gMFI, mean with SD. Each dot represents a different donor. The statistical significance between conditions was assessed by a mixed-effects model followed by Dunnett's post hoc multiple comparisons test. (D) The proliferation of allogenic CD8 and CD4 T cells was measured after co-culture for 6 days with sorted CD14$^+$ and CD14$^-$ populations (which had previously been co-cultured with PDTOs). The percentage of proliferating T cells was assessed based on CFSE staining. Scattered dot plots show the percentage of proliferating T cells in each condition, three technical replicates per donor, mean with SEM. The statistical significance was evaluated using a paired sample *t*-test. (F) The supernatants corresponding to the allogenic T-cell assay of panel (D) were collected, and the presence of IFN-γ and TNF-α was quantified using a flow cytometry-based cytokine multiplex array. Statistical significance annotated as *$p < 0.05$, **$p < 0.01$, ***$p < 0.001$, and ***$p < 0.0001$.
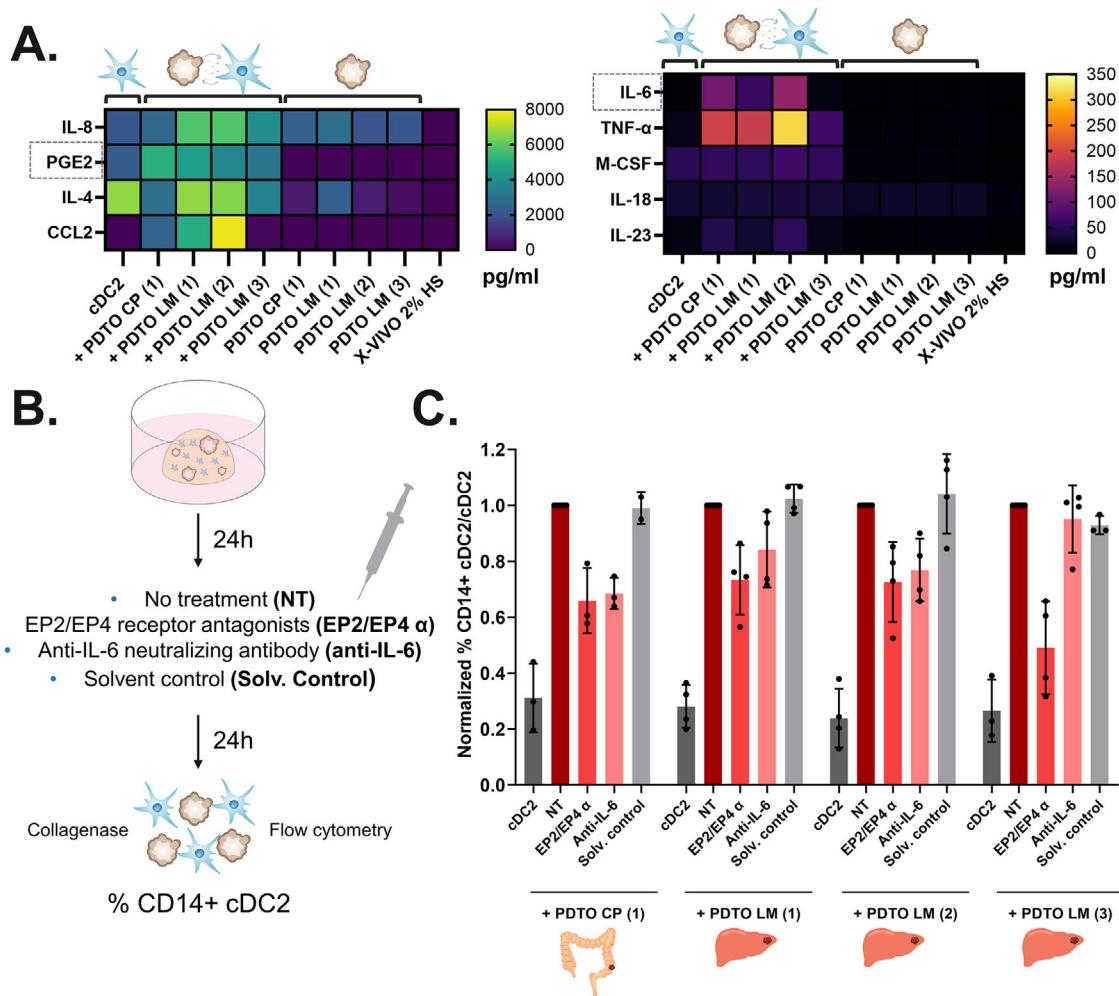
Figure 6. Characterization and inhibition of soluble factors in the 3D co-culture system. (A) A flow cytometry-based multiplex inflammatory cytokine array and ELISAs were used to screen supernatants of cDC2-PDTOs co-cultures ($n = 8$) as well as cDC2 and PDTOs cultured separately. Values for each soluble factor were plotted in heatmaps in pg/mL. (B) Schematic representation of the workflow followed to assess the impact of the anti-IL-6 neutralizing antibody and the EP2 and EP4 receptor antagonists on the percentage and phenotype of CD14$^+$ cDC2. (C) The effect of the inhibitors on the % of the CD14$^+$ cDC2 population was plotted as the fold change between the nontreated cDC2 and PDTOs condition and all the other conditions. Data plotted as normalized percentages, mean with SD. Each dot represents a different donor. The statistical significance between conditions was assessed by an ordinary one-way ANOVA followed by a Bonferroni post hoc multiple comparisons test. Statistical significance was annotated as follows: **$p < 0.01$, ***$p < 0.001$, ****$p < 0.0001$.

gating the continuous, dynamic, and reciprocal crosstalk between human cDC2 and PDTOs. Given the complexity and heterogeneity of CRC, PDTOs serve as a powerful tumor model. Organoids offer a unique window into the tumor, as they retain and represent its structure, heterogeneity, and treatment responsiveness while allowing for in vitro studies [38–41]. Additionally, even though it is challenging to isolate and work with human primary DCs, in our system blood-derived cDC2 remain adequately viable, within the expected range, and are able to perform their functions. Our results show that cDC2 were able to dynamically interact with the organoids reinforcing the physiological suitability of the system.

Upon co-culture with the PDTOs, two populations are clearly distinguishable: a CD14$^+$ and a CD14$^-$ CD1c$^+$ population, with distinct phenotypes and functions. On the one hand, the CD14$^-$ fraction expressed high activation markers, such as CD86, and

was able to trigger T-cell proliferation and pro-inflammatory cytokine release. On the other hand, the CD14+ fraction presented a mixed phenotype, simultaneously expressing cDC2 and monocyte/macrophage markers, and had impaired T-cell activating abilities. In this way, our results corroborate the plasticity and putative dual roles of this subset in antitumor immunity. Moreover, we conclude that the PDTOs stir the initial cDC2 population into two directions by concurrently activating the CD14$^-$ fraction and inducing a CD14$^+$ population with immunosuppressive properties.

The CD14$^+$ cDC2 population that emerges in our model, is also seen in other in vitro models, both in 2D and 3D, arising from human cDC2 in the presence of recombinant tumor-derived factors, tumor-conditioned medium or tumor cells [28, 35]. Interestingly, our relatively simple model shows the same

results as more laborious and complex 3D models, such as the melanoma skin model [35], while allowing us the possibility to study patient/tumor-specific effects. Our results indicate that this CD14$^+$ cDC2 population is also present in the circulation and at the tumor site of metastatic CRC patients. This is supported by multiple studies that describe this population as associated with treatment unresponsiveness and poor prognosis across different tumors [12, 24–27]. A specific study has linked DC3, identified as a cluster of cDC2 cells expressing CD1c, CD163, and CD14, to malignancy and an unfavorable prognosis among patients with CRC [25]. All in all, this phenotypic switch in cDC2 seems to be one of the mechanisms employed by (CRC) tumors to disrupt the immune system with repercussions to antitumor immunity and therapy efficacy.

Remarkably, this in vitro CD14$^+$ cDC2 tumor-induced population resembles the recently defined DC3 subset with high expression of CD14, CD163, MerTK, and CD11b, and concomitantly low expression of activation markers (CD86) and antigen-presenting machinery (HLA-DR). Due to their intermediate phenotype, debate is still ongoing in the field regarding DC3 ontogeny, functional features, nomenclature, classification, and role in diseases [29–33]. Importantly, a comparison between primary blood DC3 and CD1c$^+$ CD14$^+$ cells infiltrating breast tumors confirmed alignment in both their phenotype and transcriptome [29].

Some studies have shown that DC3 can arise independently from the common DC progenitor that originates cDC1 and cDC2 [29, 34]. Our study and others suggest that cDC2 can shift toward a DC3-like phenotype triggered by tumor-released cues, at least in vitro [28, 35]. In similar settings using the tumor-conditioned medium, unlike cDC2, monocytes failed to differentiate into DC3-like cells or acquire CD1c expression [28]. Furthermore, the data suggest that the gradual adoption by the plastic cDC2 of a DC3(-like) phenotype is relevant to cancer immunity, involving impaired T-cell activation capacity [28, 35]. This transition promotes tolerance, and immunosuppression, and ultimately facilitates tumor evasion. Given the plasticity and relevance of cDC2, further research is needed toward the development of strategies to counteract and prevent this tumor-derived effect. Altogether these findings propose an alternative, additional route by which DC3 might arise from cDC2 in the tumor setting. We propose that DC3(-like) cells in patients might originate from an independent progenitor or from cDC2.

In our study, we noted that these CD14$^+$ cDC2 cells were distributed homogeneously through the co-culture and were not restricted to the proximity of the tumor organoids. The fact that this population also arises in the presence of tumor cell line-conditioned medium as described in other studies [28] and that these cells are also found in circulation in patients' blood, suggests the role and effect of tumor-released soluble factors. Strikingly, IL-6 and many other relevant cytokines and inflammatory factors were expressed at higher levels in cDC2–PDTO co-cultures, than when compared with either monoculture.

Moreover, we noticed distinct secretome profiles generated by the co-culture with different tumor organoids. This can poten-

tially be linked to their respective genotypic and phenotypic landscapes and may translate to tumor/organoid-specific mediators and mechanisms for DC disruption. For instance, PDTO LM (3), which in general secreted lower amounts of the inflammatory factors including no or low IL-6 secretion, was also the tumor organoid with a less powerful induction of CD14+ cDC2. As the role of IL-6 in CD14+ cDC2 in vitro induction was demonstrated using recombinant IL-6 [28, 35], this emphasizes the importance of the direct co-culture setting. Indeed, a setting that allows physical interaction, dynamic crosstalk, and the continuous secretion of factors by the two cell types is more physiologically relevant and closer to the tumor context than 2D setups that make use of tumor cell line-derived conditioned medium.

In order to test the suitability of our model to assess potential therapies and to explore the possibility of reverting or preventing this undesirable tumor-driven effect, three inhibitors were tested. We decided to focus our attention on two factors — IL-6 and PGE2 — for the following reasons: (1) both were expressed in higher amounts in co-culture, (2) previous in vitro studies had shown the involvement of these factors in the induction of this population in other tumors [28, 35], and (3) several studies have confirmed the pro-tumorigenic and pro-metastatic roles of these factors in CRC [47–51].

We used inhibitors with different modes of action, an anti-IL-6 antibody to hamper the IL-6 activity, and EP2 and EP4 receptor antagonists to block PGE2 effects [35, 43]. Our results show that at the concentrations used it is possible to partially reduce the tumor-induced CD14$^+$ cDC2 population. It is noteworthy that despite the use of both inhibitors individually or simultaneously, a full restoration of this population was not achieved. This could be attributed to the continuous production of factors by cDC2 and tumor organoids, to the continuous turnover of soluble mediators, or to receptor internalization upon binding, which might require the use of higher concentrations or refreshment of inhibitors. These data align with prior research, emphasizing the influence of recombinant IL-6 and PGE2 in driving the transition of cDC2 cells toward the CD14$^+$ CD1c$^+$ phenotype. Moreover, it underscores the absence of a substantial cumulative effect previously observed upon combining both recombinant IL-6 and PGE2 [35].

Alternatively, it suggests the involvement of additional factors besides IL-6 and PGE2, which is supported by previous studies revealing the role of M-CSF (in melanoma) in inducing this population [28]. Moreover, the treatments were added 24 h after initial co-culture, meaning some cells had possibly already transitioned into a DC3-like tumor-induced phenotype, and, as previously demonstrated, this conversion is not easily reverted [28]. Furthermore, not all co-cultures responded similarly to the inhibitors, and these effects seemed to correlate to the expression level of the corresponding cytokine. Overall, we conclude that IL-6 and PGE2 contribute to the shift of cDC2 toward a DC3 phenotype. Additionally, this means that our model might be suitable for testing therapies.

Conclusion and Future Perspectives

In summary, our results imply that the presented 3D CRC-cDC2 co-culture system is robust, reproducible, and physiologically relevant, contributing to the untangling of the CRC-employed mechanisms that regulate cDC2 plasticity and function. Moreover, we hypothesize that our system allows us to study cDC2–CRC interactions in a PDTO-specific context, paving the way for personalized and patient-tailored therapeutic strategies. This points us toward the potential of this model for the design and testing of tumor- and cDC2-specific interventions to tackle the arising of this cDC2-derived DC3 population and associated detrimental consequences for antitumor immunity and treatment response.

Further research is required to strengthen the parallel between the co-culture model and patient data by correlating in vitro observations with the corresponding patient data (including disease progression and treatment response). This will also support the predictive power of this setup as a testing platform for patient-tailored medicine. Moreover, additional work is necessary to establish the ideal concentrations of treatments for maximizing drug efficacy and selectivity while minimizing potential off-target effects. Our model can then potentially be further explored for in-depth patient/tumor/mutation-specific studies concerning the (1) underlying mechanisms and mediators involved and (2) the design and testing of (combinatorial) therapies [4]. Moreover, our methods and study also set the ground for high-end translational studies, which can use treatment effectiveness by assessing the ability of cDC2 to stimulate cytotoxic antigen-specific T-cell responses, after being in co-culture with the PDTOs with and without treatment.

In addition, it remains to be elucidated whether cDC2 can indeed give rise to bona fide DC3 or solely shift toward a DC3-like state triggered by tumor-released cues as a result of the high plasticity of these cells. Further research is needed to fully understand the relationships and differences between these populations, as well as their exact functions in tumor immunity, and to determine their potential as targets for cancer immunotherapy.

Further in the future, potentially our model could also help delineate the individual contributions and involvements of other primary DC subsets (pDC and cDC1) in CRC immunity. In addition, our model can serve as a valuable resource for the identification of potential targets and biomarkers to direct cancer immunotherapies. Toward that goal, and to increase the complexity of the system, other cell types, such as lymphocytes or fibroblasts, could be included to better reflect the multicellular composition of the TME. It is important to bear in mind that mimicking the CRC TME in 3D cultures is complex, and will involve compromises in terms of feasibility, cell types, and ratios. Decisions in this regard can be aided by the study of representative patient tissue samples and sections. All in all, further exploitation of this approach can bring us closer to making existing or new immunotherapies available for more mCRC patients.

Author contributions:　Beatriz Subtil: Performed the experiments, analyzed the data, and wrote the manuscript. Jorge Cuenca-Escalona, Anouk M. D. Becker, and Mar Alvarez-Begue: Assisted with the establishment of protocols/experimental design, performing experiments, and data analysis. Iris A. E. van der Hoorn and Mark A. J. Gorris: Performed/assisted with triplex immunohistochemistry experiments in patient samples. Kirti K. Iyer, Jorien Janssen, and Dennis Poel: Established and provided essential biological material. Tom van Oorschot: Performed flow cytometry-based multiplex cytokine array assays. Jorge Cuenca-Escalona, Koen van den Dries, and Alessandra Cambi: Assisted with experimental setup, data analysis, and interpretation. Jolanda M. de Vries and Daniele V. F. Tauriello: Supervised the entire project. All authors read and approved the final manuscript.

References

1　**Morgan, E., Arnold, M., Gini, A., Lorenzoni, V., Cabasag, C. J., Laversanne, M., Vignat, J., et al.,** Global burden of colorectal cancer in 2020 and 2040: incidence and mortality estimates from GLOBOCAN. *Gut* 2023. **72**: 338–344.

2　**Rawla, P., Sunkara, T. and Barsouk, A.,** Epidemiology of colorectal cancer: incidence, mortality, survival, and risk factors. *Prz Gastroenterol.* 2019. **14**: 89–103.

3　**Sawicki, T., Ruszkowska, M., Danielewicz, A., Niedźwiedzka, E., Arłukowicz, T. and Przybyłowicz, K. E.,** A review of colorectal cancer in terms of epidemiology, risk factors, development, symptoms and diagnosis. *Cancers (Basel)* 2021. **13**.

4 Janssen, E., Subtil, B., De La Jara Ortiz, F., Verheul, H. M. W. and Tauriello, D. V. F., Combinatorial immunotherapies for metastatic colorectal cancer. *Cancers (Basel)* 2020. **12**: 1–29.

5 Kartikasari, A. E. R., Huertas, C. S., Mitchell, A. and Plebanski, M., Tumor-induced inflammatory cytokines and the emerging diagnostic devices for cancer detection and prognosis. *Front. Oncol.* 2021. **11**: 1.

6 Kamal, Y., Schmit, S. L., Frost, H. R. and Amos, C. I., The tumor microenvironment of colorectal cancer metastases: opportunities in cancer immunotherapy. *Immunotherapy* 2020. **14**: imt–2020–0026.

7 Pedrosa, L., Esposito, F., Thomson, T. M. and Maurel, J., The tumor microenvironment in colorectal cancer therapy. *Cancers (Basel)* 2019. **11**: 1172.

8 Subtil, B., Cambi, A., Tauriello, D. V. F. and De Vries, I. J. M., The Therapeutic potential of tackling tumor-induced dendritic cell dysfunction in colorectal cancer. *Front. Immunol.* 2021. **12**: 4048.

9 Lin, A., Schildknecht, A., Nguyen, L. T. and Ohashi, P. S., Dendritic cells integrate signals from the tumor microenvironment to modulate immunity and tumor growth. *Immunol. Lett.* 2010. **127**: 77–84.

10 Lucarini, V., Melaiu, O., Tempora, P., D'amico, S., Locatelli, F. and Fruci, D., Dendritic cells: behind the scenes of t-cell infiltration into the tumor microenvironment. *Cancers (Basel)* 2021. **13**: 1–22.

11 Gessani and Belardelli, Immune dysfunctions and immunotherapy in colorectal cancer: the role of dendritic cells. *Cancers (Basel)* 2019. **11**: 1–17.

12 Michea, P., Noël, F., Zakine, E., Czerwinska, U., Sirven, P., Abouzid, O., Goudot, C., et al., Adjustment of dendritic cells to the breast-cancer microenvironment is subset specific. *Nat. Immunol.* 2018. **19**: 885–897.

13 Guilliams, M. and Merad, M., Expanding dendritic cell nomenclature. **0123456789**: 2–3.

14 Segura, E., Human dendritic cell subsets: an updated view of their ontogeny and functional specialization. *Eur. J. Immunol.* 2022. **52**: 1759–1767.

15 Lizée, G. and Gilliet, M., Human dendritic cells in cancer. *Innate Immune Regul. Cancer Immunother.* 2022. **9409**: 121–145.

16 Anderson, D. A., Dutertre, C.-A., Ginhoux, F. and Murphy, K. M., Genetic models of human and mouse dendritic cell development and function. *Nat. Rev. Immunol.* 2021. **21**: 101–115.

17 Murphy, T. L. and Murphy, K. M., Dendritic cells in cancer immunology. *Cell Mol. Immunol.* 2022. **19**: 3–13.

18 Del Prete, A., Salvi, V., Soriani, A., Laffranchi, M., Sozio, F., Bosisio, D. and Sozzani, S., Dendritic cell subsets in cancer immunity and tumor antigen sensing. *Cell Mol. Immunol.* 2023. **20**: 432–447.

19 Collin, M. and Bigley, V., Human dendritic cell subsets: an update. https://doi.org/10.1111/imm.12888.

20 Segura, E., Human dendritic cell subsets: an updated view of their ontogeny and functional specialization. *Eur. J. Immunol.* 2022. **52**: 1759–1767.

21 Saito, Y., Komori, S., Kotani, T., Murata, Y. and Matozaki, T., The role of type-2 conventional dendritic cells in the regulation of tumor immunity. *Cancers (Basel)* 2022. **14**.

22 Cheng, S., Li, Z., Gao, R., Xing, B., Gao, Y., Yang, Y., Qin, S., et al., A pan-cancer single-cell transcriptional atlas of tumor infiltrating myeloid cells. *Cell* 2021. **184**: 792–809.e23.

23 Wculek, S. K., Cueto, F. J., Mujal, A. M., Melero, I., Krummel, M. F. and Sancho, D., Dendritic cells in cancer immunology and immunotherapy. *Nat. Rev. Immunol.* 2020. **20**: 7–24.

24 Bakdash, G., Buschow, S. I., Gorris, M. A. J., Halilovic, A., Hato, S. V., Sköld, A. E., Schreibelt, G., et al., Expansion of a BDCA1+ CD14+ myeloid cell population in melanoma patients may attenuate the efficacy of dendritic cell vaccines. *Cancer Res.* 2016. **76**: 4332–4346.

25 Liu, Y., Zhang, Q., Xing, B., Luo, N., Gao, R., Yu, K., Hu, X., et al., Immune phenotypic linkage between colorectal cancer and liver metastasis. *Cancer Cell* 2022: 1–14.

26 Laoui, D., Keirsse, J., Morias, Y., Van Overmeire, E., Geeraerts, X., Elkrim, Y., Kiss, M., et al., The tumour microenvironment harbours ontogenically distinct dendritic cell populations with opposing effects on tumour immunity. *Nat. Commun.* 2016. **7**: 1–17.

27 Segura, E., Touzot, M., Bohineust, A., Cappuccio, A., Chiocchia, G., Hosmalin, A., Dalod, M., et al., Human inflammatory dendritic cells induce Th17 cell differentiation. *Immunity* 2013. **38**: 336–348.

28 Becker, A.M.D., Decker, A.H., Flórez-Grau, G., Bakdash, G., Röring, R.J., Stelloo, S., Vermeulen, M., et al., Inhibition of CSF-1R and IL-6R prevents conversion of cDC2s into immune incompetent tumor-induced DC3s boosting DC-driven therapy potential. *Cell Reports Med.* 2024. **5**.

29 Bourdely, P., Anselmi, G., Vaivode, K., Ramos, R.N., Missolo-Koussou, Y., Hidalgo, S., Tosselo, J., et al., Transcriptional and functional analysis of CD1c+ human dendritic cells identifies a CD163+ subset priming CD8+CD103+ T cells. *Immunity* 2020. **53**: 335–352.e8.

30 Alcántara-Hernández, M., Leylek, R., Wagar, L.E., Engleman, E.G., Keler, T., Marinkovich, M.P., Davis, M. M., et al., High-dimensional phenotypic mapping of human dendritic cells reveals interindividual variation and tissue specialization. *Immunity* 2017. **47**: 1037–1050.e6.

31 Villani, A.-C., Satija, R., Reynolds, G., Sarkizova, S., Shekhar, K., Fletcher, J., Griesbeck, M., et al., Single-cell RNA-seq reveals new types of human blood dendritic cells, monocytes and progenitors. *Science* 2017. **356**.

32 Dutertre, C.-A., Becht, E., Irac, S. E., Khalilnezhad, A., Narang, V., Khalilnezhad, S., Ng, P. Y., et al., Single-cell analysis of human mononuclear phagocytes reveals subset-defining markers and identifies circulating inflammatory dendritic cells. *Immunity* 2019. **51**: 573–589.e8.

33 Gerhard, G. M., Bill, R., Messemaker, M., Klein, A. M. and Pittet, M. J., Tumor-infiltrating dendritic cell states are conserved across solid human cancers. *J. Exp. Med.* 2021. **218**.

34 Cytlak, U., Resteu, A., Pagan, S., Green, K., Milne, P., Maisuria, S., Mcdonald, D., et al., Differential IRF8 transcription factor requirement defines two pathways of dendritic cell development in humans. *Immunity* 2020. **53**: 353–370.e8.

35 Di Blasio, S., Van Wigcheren, G. F., Becker, A., Van Duffelen, A., Gorris, M., Verrijp, K., Stefanini, I., et al., The tumour microenvironment shapes dendritic cell plasticity in a human organotypic melanoma culture. *Nat. Commun.* 2020. **11**: 1–17.

36 Subtil, B., Iyer, K. K., Poel, D., Bakkerus, L., Gorris, M. A. J., Escalona, J. C., Dries, K. V. D., et al., Dendritic cell phenotype and function in a 3D co-culture model of patient-derived metastatic colorectal cancer organoids. *Front. Immunol.* 2023. **14**: 1–13.

37 Iyer, K. K. and Poel, D., High-dose short-term osimertinib treatment is effective in patient-derived metastatic colorectal cancer organoids. *Research Square* 2023: 1–25.

38 Yuan, J., Li, X. and Yu, S., Cancer organoid co-culture model system : novel approach to guide precision medicine. *Front. Immunol.* 2023.

39 Kim, J., Koo, B.-K. and Knoblich, J. A., Human organoids: model systems for human biology and medicine. *Nat. Rev. Mol. Cell Biol.* 2020. **21**: 571–584.

40 Ooft, S. N., Weeber, F., Dijkstra, K. K., Mclean, C. M., Kaing, S., Van Werkhoven, E., Schipper, L., et al., Patient-derived organoids can predict response to chemotherapy in metastatic colorectal cancer patients. *Sci. Transl. Med.* 2019. **11**.

41 **Yuki, K., Cheng, N., Nakano, M. and Kuo, C. J.,** Organoid models of tumor immunology. *Trends Immunol.* 2020. **41**: 652–664.

42 **Koh, W. H., Zayats, R., Lopez, P. and Murooka, T. T.,** Visualizing cellular dynamics and protein localization in 3D collagen. *STAR Protoc.* 2020. **1**: 100203.

43 **Cuenca-Escalona, J., Flórez-Grau, G., Van Den Dries, K., Cambi, A. and De Vries, I. J. M.,** PGE2-EP4 signaling steers cDC2 maturation towards the induction of suppressive T cell responses. *Eur. J. Immunol.* 2023. https://doi.org/10.1002/EJI.202350770.

44 **Gorris, M. A. J., Van Der Woude, L. L., Kroeze, L. I., Bol, K., Verrijp, K., Amir, A. L., Meek, J., et al.,** Paired primary and metastatic lesions of patients with ipilimumab-treated melanoma: high variation in lymphocyte infiltration and HLA-ABC expression whereas tumor mutational load is similar and correlates with clinical outcome. *J. Immunother. Cancer* 2022. **10**: e004329.

45 **Van Der Hoorn, I. A. E., Martynova, E., Subtil, B., Meek, J., Verrijp, K., Textor, J., Flórez-Grau, G., et al.,** Detection of dendritic cell subsets in the tumor microenvironment by multiplex immunohistochemistry. *Eur. J. Immunol.* 2024. **54**: e2350616.

46 **Gorris, M. A. J., Halilovic, A., Rabold, K., Van Duffelen, A., Wickramasinghe, I. N., Verweij, D., Wortel, I. M. N., et al.,** Eight-color multiplex immunohistochemistry for simultaneous detection of multiple immune checkpoint molecules within the tumor microenvironment. *J. Immunol.* 2018. **200**: 347–354.

47 **Wang, F., Wang, M., Yin, H., Long, Z., Zhu, L., Yu, H., Sun, H., et al.,** Association between plasma prostaglandin E2 level and colorectal cancer. *Eur. J. Cancer Prev.* 2021. **30**: 59–68.

48 **Bhat, A. A., Nisar, S., Singh, M., Ashraf, B., Masoodi, T., Prasad, C. P., Sharma, A., et al.,** Cytokine- and chemokine-induced inflammatory colorectal tumor microenvironment: emerging avenue for targeted therapy. *Cancer Commun.* 2022. **42**: 689–715.

49 **Zafari, N., Khosravi, F., Rezaee, Z., Esfandyari, S., Bahiraei, M., Bahramy, A., Ferns, G. A., et al.,** The role of the tumor microenvironment in colorectal cancer and the potential therapeutic approaches. *J. Clin. Lab. Anal.* 2022. **36**.

50 **Mager, L. F., Wasmer, M.-H., Rau, T. T. and Krebs, P.,** Cytokine-induced modulation of colorectal cancer. *Front. Oncol.* 2016. **6**: 96.

51 **Toyoshima, Y., Kitamura, H., Xiang, H., Ohno, Y., Homma, S., Kawamura, H., Takahashi, N., et al.,** IL6 modulates the immune status of the tumor microenvironment to facilitate metastatic colonization of colorectal cancer cells. *Cancer Immunol. Res.* 2019. **7**: 1944–1957.

Abbreviations: **cDC2**: conventional dendritic cell type 2 · **CEA**: carcinoembryonic antigen · **CP**: colon primary · **CRC**: colorectal cancer · **DC**: dendritic cell · **FACS**: fluorescence-activated cell sorting · **HUB**: Hubrecht Organoid Technology · **LM**: liver metastasis · **M-CSF**: macrophage colony-stimulating factor · **PanCK**: pancytokeratin · **PDTOs**: patient-derived tumor organoids · **PGE2**: prostaglandin E2 · **TME**: tumor microenvironment

Full correspondence: Dr. I. Jolanda M. de Vries, Radboud University Medical Center, Medical BioSciences, 5th floor, Route code 278, Geert Grooteplein 26–28, 6525 GA Nijmegen, the Netherlands
e-mail: jolanda.devries@radboudumc.nl